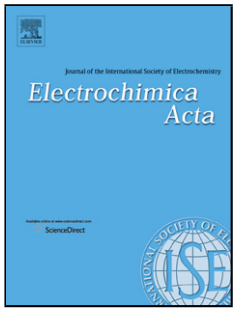

Title: Electroactive (A_3+B_2)-type hyperbranched polyimides with highly stable and multistage electrochromic behaviors

Authors: Ningwei Sun, Shiyao Meng, Ziwei Zhou, Danming Chao, Ye Yu, Kaixin Su, Daming Wang, Xiaogang Zhao, Hongwei Zhou, Chunhai Chen

PII: S0013-4686(17)32095-9
DOI: https://doi.org/10.1016/j.electacta.2017.10.036
Reference: EA 30422

To appear in: *Electrochimica Acta*

Received date: 2-5-2017
Revised date: 4-10-2017
Accepted date: 4-10-2017

Please cite this article as: Ningwei Sun, Shiyao Meng, Ziwei Zhou, Danming Chao, Ye Yu, Kaixin Su, Daming Wang, Xiaogang Zhao, Hongwei Zhou, Chunhai Chen, Electroactive (A3+B2)-type hyperbranched polyimides with highly stable and multistage electrochromic behaviors, Electrochimica Acta https://doi.org/10.1016/j.electacta.2017.10.036

Electroactive (A_3+B_2)-type hyperbranched polyimides with highly stable and multistage electrochromic behaviors

Ningwei Sun,[a1] Shiyao Meng,[a1] Ziwei Zhou,[b1] Danming Chao,[a] Ye Yu,[c] Kaixin Su,[a] Daming Wang,[a] Xiaogang Zhao,[a] Hongwei Zhou[a] *and Chunhai Chen[a]

Corresponding author: Hongwei Zhou

Email address: zhw@jlu.edu.cn

[a] Alan G. MacDiarmid Institute of Jilin University, Changchun 130012, P. R. China

[b] State Key Laboratory of Supramolecular Structure and Materials, Jilin University, Changchun 130012, P.R. China

[c] Leibniz Institut für Polymerforschung Dresden e.V, Institute of Physical Chemistry and Polymer Physics, Hohe Str. 6, D-01005, Dresden, Germany

Graphical Abstract

Novel hyperbranched polyimides with star-shaped triphenylamine were synthesized, which exhibited multistage visible/near-infrared electrochromic and supercapacitive properties.

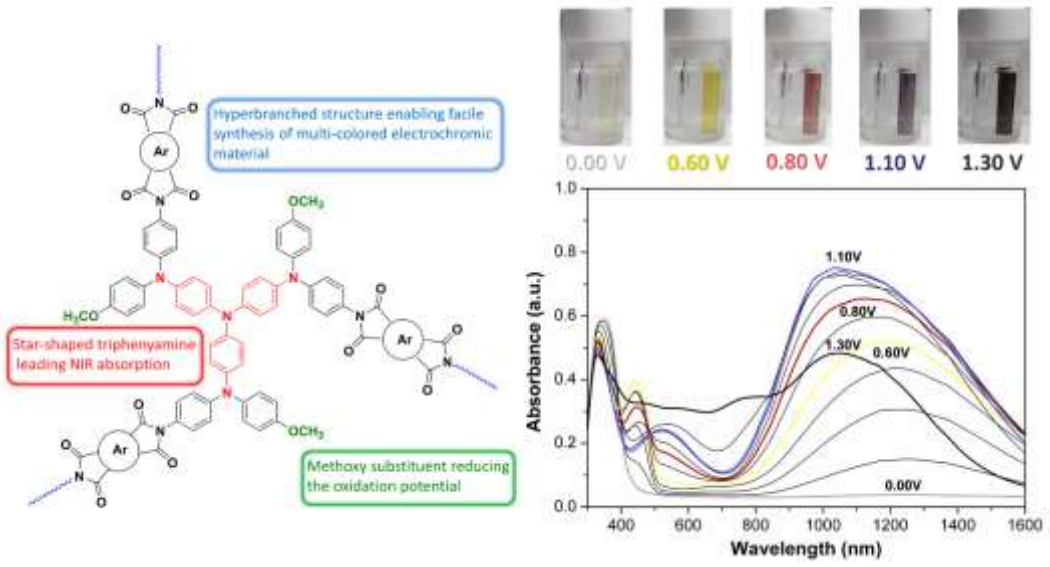

[1] The authors contributed equally to this work.

Abstract

Multicolored electrochromic materials have attracted intense attentions due to their diverse smart applications. In this work, we demonstrate a facile strategy to realize multistage visible/near-infrared (vis/NIR) electrochromism by designing and synthesizing two kinds of novel hyperbranched polyimides (HBPIs) from a novel triamine as an A_3 monomer and two dianhydrides as B_2 monomers. The resulting HBPIs exhibit excellent solubility and thermostability. Cyclic voltammograms of the HBPIs films reveal four reversible redox couples along with five color conversions (colorless-yellow-red-indigo-black). Furthermore, the HBPIs exhibit superb electrochromic performances including continuous modulation over the entire visible region, short response time, high optical contrast, high coloration efficiency, excellent switching stability and long-term optical memory. Accordingly, these HBPIs are promising materials in the applications of electrochromism and even endowing difunctionality combining with supercapacitance.

Keywords: HBPIs; Triphenylamine; Multi-electrochromism

1. Introduction

Electrochromic materials with redox-active species achieve reversible changes in absorption/transmittance upon electrical stimulus. The controllable optical properties of electrochromic materials have garnered increasing interest spanning the field of smart windows, displays, sunglasses, anti-glare rear-view mirrors and camouflage materials [1-7]. Compared with traditional inorganic oxides, the organic electrochromic materials possess numerous advantages, including facile processability, fast switching time, high coloration efficiency and fine-tuning of the band gap with structure modification [8-14]. Early studies of electrochromic materials mainly focused

on the change of visible light. Recently, the field of modulation of near-infrared light has also received great attention, and the NIR electrochromism is desirable for thermal control in buildings or spacecraft, data storage and optic-fiber communication [15-17]. Various materials including conjugated polymers, cyclometalated complexes, composites of transition metal oxide (TMO)-nanocrystal and derivatives with *p*-phenylenediamine structures have been exploited as NIR electrochromic materials [18-26]. Additionally, electrochromo-supercapacitors bridging the gap between the electrochromism and energy storage are attracting scientists' interest due to their smartness and integration [27-29]. Yet to meet the requirements of commercial applications, there are still some crucial factors need to be improved including high optical contrast, long-term stability, high specific capacitance and facile processing technology, which will greatly promote the development of versatile materials.

Triphenylamine derivatives with fascinating photo- and electro-active properties have been widely applied in organic solar cells, hole transporters, organic light emitting diodes (OLEDs) and memory devices [30-35]. Moreover, triphenylamine-containing polymers have been recently developed as attractive electrochromic materials due to their facial oxidation to corresponding radical cations; the redox process is highly stable as long as the *para*-position of triphenylamine is protected by electron-donating substituent such as methoxy group [36-43]. Generally, the more electroactive species of triphenylamine were introduced, the more stages of electrochromism occurred during the redox process [44-46]. However, it is difficult to introduce more than two electroactive species for traditional linear materials because of the intricate multi-step synthetic procedures. To overcome this limitation, synthesis of hyperbranched polymers containing star-shaped triphenylamine will be an effective and facile method. The trifunctional monomer could be imparted with three electroactive triphenylamine

through a one-step synthesis, which will greatly simplify the synthesis and purification technique. Moreover, the unique loose packing of hyperbranched architecture could enable a fast redox process and enhance the optical response stability by facilitating the ion insert/extraction [47-49].

In this work, we describe two kinds of novel (A_3+B_2)-type hyperbranched polyimides (HBPIs) with a new triamine containing star-shaped triphenylamine, "4, 4', 4''-tris[4-aminophenyl(4-methoxyphenyl)amino]triphenylamine", as an A_3 monomer and two dianhydrides as B_2 monomers. Introducing star-shaped triphenylamine with *para*-substituted methoxy group along the HBPI backbone is expected to obtain superior electrochromic materials with excellent integrated performances, such as low response time, multistage modulations in the vis/NIR regions, low trigger voltage and high stability. Moreover, the capacitive properties of the HBPIs were also initially investigated to explore their potential application as smart supercapacitors.

Figure 1

2. Experimental section

2.1 Materials

Tris(4-iodophenyl)amine (TCI), 4-fluoronitrobenzene (Acros), 4-methoxyaniline (TCI), potassium carbonate (TCI), copper powder (Acros), 18-crown-6-ether (TCI), triethylamine (Acros), hydrazine monohydrate (TCI), 10% palladium on charcoal (Pd/C, TCI), acetic anhydride (TCI) were used as received. *N*-methyl-2-pyrrolidinone (NMP), dimethyl sulfoxide (DMSO), *o*-dichlorobenzene (TCI) and pyridine (Acros) were dried using 4 Å molecular sieves prior to use. Commercially available tetracarboxylic dianhydrides including 3,3',4,4'-

oxydiphthalic anhydride (ODPA, TCI) and 2,2-bis(3,4-dicarboxyphenyl)hexafluoropropane dianhydride (6FDA, TCI) were used after being dried under vacuum at 140 °C for 12 h. Tetrabutylammonium perchlorate (TBAP, Acros) was recrystallized twice from ethanol under nitrogen atmosphere and then dried under vacuum before use. All other commercially available reagents and chemicals were used without further purification.

2.2 Synthesis of 4-Methoxy-4'-nitrodiphenylamine

4-Methoxy-4'-nitrodiphenylamine was synthesized according to the reported procedure [38] with simple modifications. In a 1000 mL three-neck round-bottom flask, a mixture of 60.0 g (487.5 mmol) 4-methoxyaniline, 52.9 g (375.0 mmol) 4-fluoronitrobenzene, 50.0 g (487.5 mmol) triethylamine and 350 mL dried DMSO was heated at 90 °C for 36 h under nitrogen atmosphere. After cooling to ambient temperature, the mixture was poured into ice water to precipitate orange powder. Then the crude product was recrystallized from DMSO/ethanol (1:3) to give orange needle crystals (82 % of yield, mp=156 °C, literature [38] 153 °C by DSC at 10 °C/min). ^{1}H NMR (300 MHz, DMSO-d_6, δ, ppm): 9.12 (s, 1H), 8.05 (d, J = 9.3 Hz, 2H), 7.18 (d, J = 8.9 Hz, 2H), 6.98 (d, J = 8.9 Hz, 2H), 6.88 (d, J = 9.3 Hz, 2H), 3.76 (s, 3H).

2.3 Synthesis of "4, 4', 4''-tris[4-nitrophenyl(4-methoxyphenyl) amino]triphenylamine

To a 250 mL round-bottom flask equipped with a stirring bar, 10.0 g (16.0 mmol) of tris(4-iodophenyl)amine, 17.6 g (72.0 mmol) of 4-methoxy-4'-nitrodiphenylamine, 6.1 g (96.0 mmol) of copper powder, 13.3 g (96.0 mmol) of K_2CO_3 and 2.5 g (9.6 mmol) of 18-crown-6-ether were added along with 50 mL dried *o*-dichlorobenzene, which were then stirred at 180 °C for 24 h under nitrogen atmosphere. Then, the reaction mixture was immediately

filtered, and the filtrate was cooled down to room temperature to precipitate red powder. The crude product was recrystallized from DMF/ethanol (2:1) to obtain 13.0 g of trinitro compound (83% yield, mp=271 °C). FT-IR (KBr): 1310 cm^{-1}, 1582 cm^{-1}(-NO_2 stretch). ^{1}H NMR (300 MHz, DMSO-d_6, δ, ppm): 8.05 (d, J = 9.3 Hz, 6H, H_a), 7.37–7.20 (m, 12H, H_e+H_c), 7.13 (d, J = 8.9 Hz, 6H, H_f), 7.05 (d, J = 8.8 Hz, 6H, H_d), 6.75 (d, J = 9.2 Hz, 6H, H_b), 3.79 (s, 9H, -OCH_3). ^{13}C NMR (75 MHz, DMSO-d_6, δ, ppm): 157.78, 153.78, 144.48, 139.86, 138.28, 137.34, 128.82, 127.76, 125.58, 125.05, 115.57, 115.39, 55.35.

2.4 Synthesis of "4, 4', 4''-tris[4-aminophenyl(4-methoxyphenyl) amino]triphenylamine

In a 500 mL round-bottom flask equipped with a stirring bar, 6.0 g (6.2 mmol) of trinitro compound and 1.0 g of 10% Pd/C were dispersed in 150 mL of 1,4-dioxane. After heating the suspension solution to reflux, 15.5 g of hydrazine monohydrate was added to the mixture slowly. Then the mixture was stirred at the reflux temperature for further 48 h. Pd/C was removed by immediately filtered, and the filtrate was cooled under a nitrogen flow to grow faint yellow crystals. The crystals were collected by filtration and dried under vacuum at 80 °C, yielding 3.9 g of the desired triamine compound in 71 % with a melting point of 265 °C. FT-IR (KBr): 3369 cm^{-1}, 3446 cm^{-1}(-NH_2 stretch). ^{1}H NMR (300 MHz, DMSO-d_6, δ, ppm): 7.04–6.71 (m, 24H, H_c+H_b+H_d+h_e), 6.67 (d, J = 8.9 Hz, 6H, H_f), 6.52 (d, J = 8.6 Hz, 6H, H_a), 4.99 (s, 6H, -NH_2), 3.70 (s, 9H, -OCH_3). ^{13}C NMR (75 MHz, DMSO-d_6, δ, ppm): 155.01, 145.96, 143.99, 141.65, 140.83, 136.46, 127.57, 125.10, 124.44, 121.16, 115.35, 115.06, 55.65.

Scheme 1

2.5 Synthesis of HBPIs

Two kinds of HBPIs were prepared by two-step condensation polymerizations (Scheme 2), and the resulting polymers were abbreviated to ODPA-HBPI and 6FDA-HBPI, respectively. In a typical procedure, 0.2221 g of 6FDA (0.50 mmol) was dissolved in 5.5 g of DMAc under nitrogen atmosphere, to which, the triamine (0.2203 g, 0.25 mmol) in 4.0 g DMAc was added dropwise over 1 h. The solid content of the reaction solution was about 4.5 %. After 12 h, 2 mL of acetic anhydride and 1 mL of pyridine were added to the resulting polyamic acid solution, which was heated to 120 °C and stirred for further 12 h. The resulting polymer solution was then precipitated from 200 mL of stirred methanol, and the orange precipitate was collected by filtration, washed thoroughly with ethanol, and dried under vacuum at 100 °C for 10 h and 250 °C for 2 h. FT-IR (KBr): 1378, 1720 and 1785 cm^{-1} (imide group) ^1H NMR (300 MHz, DMSO-d_6, δ, ppm): 8.09 (d, 6H), 7.89 (s, 6H), 7.70 (d, 6H), 6.95 (s, 36H), 3.71 (s, 9H).

Scheme 2

2.6 Measurements

Fourier transform infrared (FT-IR) spectra were recorded through a Bruker Vector 22 spectrometer at a resolution of 4 cm^{-1} in the range of 400-4000 cm^{-1}. Nuclear magnetic resonance (NMR) spectra were run on a BRUKER-300 spectrometer in deuterated DMSO. Weight-average molecular weights (M_w) and number-average molecular weights (M_n) were obtained *via* gel permeation chromatographic (GPC) analysis on the basis of polystyrene calibration on a PL-GPV 220 instrument with DMF as an eluent at a flow rate of 1.0 mL/min. Differential scanning calorimetric (DSC) analysis was performed on a TA instrument DSC Q100 at a scanning rate of 10 °C/min in a nitrogen flow of 50 mL/min. Thermo gravimetric analysis (TGA) in the temperature of 100-800 °C was studied on the TA 2050, with a heating

rate of 10 °C/min under nitrogen atmosphere. Cyclic voltammetry (CV), galvanostatic charge-discharge (GCD) tests and electrochemical impedance spectroscopy (ESI) were conducted in a three-electrode cell with a CHI 660e electrochemical workstation. The working electrode was prepared by drop-coating 0.1 mL of polymer solutions (3mg/mL in DMAc) onto an ITO glass substrate and then dried in vacuum (the area of polymer films is about 1 cm^2 and the thickness is about 800-900 nm). A platinum wire was used as an auxiliary electrode and an Ag/AgCl, KCl (sat.) was used as a reference electrode. 0.1 M TBAP in dried CH_3CN was used as supporting electrolyte. Ultraviolet-visible (UV-vis) spectra were measured using a Shimadzu UV 3101-PC spectrophotometer. CIE Yxy chromaticity coordinates were obtained from the software of UVPC Color Analysis. The molecular simulation of the model compound was performed at the time-dependent density functional theory (TD-DFT) with a method of the B3LYP/6-31G (d, p).

3. Results and discussion

3.1 Synthesis of monomers and HBPIs

The star-shaped triamine with four electroactive triphenylamine units was selected to prepare the HBPIs due to the simplified synthetic route of introducing multiple triphenylamine [41] and the advantages are depicted in Figure 1. The triamine was synthesized *via* a three-step route (Scheme 1): first, 4-methoxy-4'-nitrodiphenylamine was synthesized by the reaction of 4-methoxyaniline and 4-fluoronitrobenzene under triethylamine assistance; second, Ullmann reaction was employed to obtain trinitro monomer from 4-methoxy-4'-nitrodiphenylamine and tris(4-iodophenyl)amine; third, the target triamine monomer was successfully synthesized by the Pd/C-catalyzed hydrazine reduction of the trinitro monomer. The structures of the resulting

monomers were systematically analyzed and identified by FT-IR and NMR spectroscopic techniques. From the FT-IR spectra (Figure S1), we could see that the characteristic bands of nitro groups at 1582 and 1310 cm^{-1} (-NO_2 asymmetric and symmetric stretching) disappeared after reduction, and N-H stretching absorptions pairs appeared in the region of 3300-3500 cm^{-1}, meaning the formation of the target triamine. Figure 2 illustrates the ^1H NMR spectra of the trinitro and triamine monomers with the assignments for proton signals, which agree well with their target molecular structures. Furthermore, the complete transformations from nitro groups to amino groups were also supported by the high field shift of the aromatic protons and the resonance signals of amino protons at around 4.99 ppm [44]. Thus, all the spectral analyses verified that the new star-shaped triamine was successfully synthesized.

Next, as shown in Scheme 2, two kinds of HBPIs were prepared from the as-prepared star-shaped triamine and two dianhydrides (ODPA and 6FDA) through a two-step polymerization. To avoid gelation in the polymerization process [50], the triamine was added to the dianhydride slowly with a monomer molar ratio of 1:2 (the molar ration between the amino and anhydride groups was 3:4), and the resulting anhydride-terminated polyamic acids were subsequently converted into polyimides by the chemical imidization. The molecular weights of these HBPIs were determined by GPC, showing the number-average molecular weights (M_ns) in the range of 26100-30800. The FT-IR spectra of these HBPIs exhibited characteristic absorption bands at 1785 (C=O asymmetrical stretching), 1720 (C=O symmetrical stretching) and 1378 cm^{-1} (C-N stretching) without the absorption band at around 1680 cm^{-1} (polyamic acid), which indicated that these HBPIs were fully imidized (Figure S2). Furthermore, typical ^1H NMR spectrum of

6FDA-HBPI was illustrated in Figure S3 and all the proton signals were well assigned to the hydrogen atoms in the repeating unit.

Figure 2

3.2 Solubility and thermal properties

To generally reveal the inherent physical properties of the HBPIs, the solubility and thermal tests were systematically studied. The former was conducted by dissolving 10 mg of HBPI powders in 1 mL of various organic solvents, with the corresponding solubility data listed in Table 1, from which we could see that the as-prepared HBPIs exhibited excellent solubility in polar solvents such as NMP, DMAc, DMF and DMSO, bringing great benefit to the fabrication of large-scale thin film devices in practical optoelectronic applications. Notably, the 6FDA-HBPI with hexafluoroisopropylidene structure revealed even more enhanced solubility in less polar solvents like THF and $CHCl_3$. We attributed the outstanding solubility to the introduction of bulky star-shaped triphenylamine groups and the resulting loose packing of hyperbranched structure [51]. On the other hand, the thermal behaviors of the HBPIs were evaluated by DSC and TGA (Figure S4). Their glass transition temperatures were observed at 252-286 °C in the DSC curves depending on the stiffness of the polymer structures. TGA curves of the two kinds of HBPIs by heating under nitrogen atmosphere both showed excellent thermal stability with 10% weight loss in the range of 490-504 °C. Their carbonized residue at 800 °C accounted for over 53%, which could be ascribed to the high aromatic content.

Table 2

3.3 Optical and electrochemical properties

We further investigated the basic optical properties of polymer solutions and drop-cast films by UV-vis spectroscopy with the detailed data summarized in Table 2. Their absorption maxima located at ultraviolet region (315, 345 and 303, 339 nm) are attributed to the π–π* transition of star-shaped triphenylamine [42]. The optical energy band gaps (E_g) lay between 2.86 and 2.88 eV, which were estimated from λ_{onset} of the HBPI films (Figure S5). As to the electrochemical properties, CV measurements were performed to investigate the electrochemical behaviors of the trinitro monomer, triamine monomer, and HBPI films in an electrolyte solution of 0.1 M TBAP/ CH_3CN with an Ag/AgCl reference electrode and a Pt wire counter electrode. As shown in Figure 3 (a, b), the trinitro monomer exhibited four pairs of reversible redox current peak at 0.75/0.64 V, 0.94/0.84 V, 1.41/1.05 V and 1.48/1.21 V, respectively; while the triamine monomer exhibited five redox couples at 0.26/0.14 V, 0.54/0.44 V, 0.69/0.58 V, 0.93/0.71 V and 1.05/0.81 V, respectively. Given that the redox reactions are sensitive to the electronic effect of different substituents [52], the triamine monomer with electron-donating amine group was more easily oxidized in comparison with the trinitro monomer containing electron-withdraw nitro group. In the case of the HBPIs, the electronic effect of imide groups locates between those of the nitro and amine groups and thus the oxidation potentials of the HBPIs occurred moderately (Figure 3c). In the quest to identify the oxidization order of the four electroactive species in the HBPIs, TD-DFT calculation was carried out to simulate the molecular orbitals of the model compound. As depicted in Figure 3f, the highest occupied molecular orbital (HOMO) was mainly located at the center triphenylamine, while the HOMO-1 and HOMO-2 were spread over the side triphenylamines, which indicated that the electrochemical redox reaction initially occurred in the center

triphenylamine and subsequently in the side triphenylamines (Figure 3e). Accordingly, in the first oxidation stage of the CV measurement of 6FDA-HBPI (Figure 3d), corresponding to the redox process of center triphenylamine, the 6FDA-HBPI thin film exhibited a low onset potential of 0.33 V and highly reversible CV behaviors for 5000 cycles, which could be ascribed to the strong electron-donating effect of the side triphenylamine [52]. Besides, the HOMO levels of these HBPIs were estimated to be 4.77-4.78 eV on the basis of their onset oxidation potentials and ferrocene/ferrocenium reference. The corresponding lowest occupied molecular orbital (LUMO) levels were estimated by HOMO levels and E_gs [53], which were calculated to be 1.90-1.91 eV (LUMO = HOMO-E_g). Notice, however, the optical band gap may be quite different from the electrochemical band gap [54], and thus the LUMO levels were roughly estimated. All the details of electrochemical data as well as HOMO and LUMO levels were gathered in Table 2.

Figure 3

Table 2

3.4 Spectroelectrochemical analysis

Considering the interesting phenomenon that the HBPI films switched between five colors reversibly during the electrochemical oxidation, *in situ* UV-vis-NIR spectroelectrochemical measurements were performed to compare the optical properties of the HBPIs at different applied potentials. These two kinds of HBPI films exhibited similar electrochromic properties with the typical absorption optical changes of 6FDA-HBPI shown in Figure 4 (ODPA-HBPI in Figure S6). Upon the electro-oxidation steadily arising from 0.0 V to 0.6 V, the intensity of the characteristic absorption peak at 339 nm for the neutral form of 6FDA-HBPI decreased

gradually, while two new well-defined absorption bands at 443 and 1250 nm grew up, respectively. The change in visible light range was attributed to the formation of monocation radical 6FDA-HBPI $^{+}$ in the center star-shaped triphenylamine unit and the broad NIR absorption resulted from the IV-CT excitation between states in which the positive charge is centered at different N atoms [55]. As the applied potential was further increased to 0.8 V, the absorption peak at 443 nm decreased with a broad band at 446 nm and a new NIR band centered at 1080 nm emerged, corresponding to the formation of 6FDA-HBPI $^{2+}$. For the third oxidation stage from 6FDA-HBPI $^{2+}$ to 6FDA-HBPI $^{3+}$, the absorption band in the visible region shifted to 520 nm and the strong IV-CT band at 1050 nm could be still observed. When the potential was applied up to 1.3 V, the 6FDA-HBPI $^{4+}$ revealed a broad absorption in the whole visible region and the NIR absorption band decreased significantly due to the fully oxidation of four triphenylamines in 6FDA-HBPI [56]. Accordingly, the multiple electro-switchings in both visible and NIR regions were realized, and the continuous modulation covered the entire visible region. The series of spectra changes revealed a good consistence with the distinguished color changes of the 6FDA-HBPI film which switched from near colorless neutral state (CIE Yxy: 112.12, 0.3273, 0.3440) to yellow first-oxidized state (CIE Yxy: 74.64, 0.4249, 0.4793), red second-oxidized state (CIE Yxy: 35.57, 0.3957, 0.3664), indigo third-oxidized state (CIE Yxy: 26.89, 0.3382, 0.2813) and black fourth-oxidized state (CIE Yxy: 12.31, 0.3256, 0.3317) (Figure 4). Notably, the achievement of “transmissive to black” electrochromism is promising in the application of energy-efficient displays [57].

Figure 4

3.5 Electrochromic performance

To evaluate the prospects of the as-prepared HBPIs in electrochromic applications, some key parameters including stability, switching time, optical contrast, coloration efficiencies and optical memory were systematically analyzed and disclosed in detail. The electrochromic switching studies were investigated by chronoamperometric-transmittance coupling analysis with the transmittance at the given wavelengths monitored as a function of time. As shown in Figure 5, four electrochromic switching processes were investigated in the visible region. For the first two redox stages (0.00-0.60 V and 0.00-0.80 V), the 6FDA-HBPI film exhibited excellent stability for 100 continuous cycles. With the switching potential applied higher (1.10 V), the electrochromic switching stability of the polymer film started to reduce gradually. By further applying increased positive potential value up to 1.30 V, the switching stability got weaker with the optical contrast decreasing obviously. The lower switching stability may be ascribed to the electroactivity loss of the polymers at high potentials [6]. Optical contrasts during the switching processes were found to be 63%, 42%, 44% and 49%, respectively. While attaining 90% of the total transmittance change, the response time for coloring/blenching were 2.6/1.9 s, 1.8/4.3 s, 2.3/1.8 s and 4.9/3.1 s as summarized in Table 3. Compared with some liner polymers [58], the fast switching speed of 6FDA-HBPI is partly attributed to its hyperbranched architecture, which results in the favourable loose packing of the polymer chains. Moreover, the coloration efficiency (CE) is also an essential parameter for electrochromic materials, which is estimated through the following equation: CE = log ($T_{blenched}/T_{colored}$)/Q_d ($T_{blenched}/T_{colored}$: transmittance in the blenched/colored state; Q_d: charge injected/ejected into the polymer film per unit area during a redox step). The CE values of 6FDA-HBPI was calculated to be 196 $cm^2 C^{-1}$ at 430 nm, 92 $cm^2 C^{-1}$ at 430 nm, 86 $cm^2 C^{-1}$ at 520 nm, and 89 cm^2

C^{-1} at 600 nm, respectively. Additional, the optical switching of 6FDA-HBPI film in NIR region was also studied, which excellent stability for the first two redox stages consistent with the results in the visible region (Figure S7). Figure S8a depicted the long-term stability test by keeping 1000 s for the coloring/blenching processes, which also exhibited highly stable electrochromic behaviors. On the other hand, optical memory (open-circuit memory) describes the ability of a material to retain its colored state upon removing the external bias, and here, the long-term memory of 6FDA-HBPI electrochromic film was measured by monitoring the transmittance changes of open-circuit states at 1250 nm and 1080 nm after applying 0.6 V and 0.8 V for 20 s, respectively. Very slight dropping of transmittance contrast could be observed in the absence of potential for 10000 s with only 3% decay at 1250 nm and 7% decay at 1080 nm (Figure S8b). Hence, the HBPIs exhibited excellent electrochromic properties and their NIR optical modulations may endow them with a promising application in the buildings for environment control of heat gain or loss [59].

Figure 5

Table 3

3.6 Capacitive properties

The highly stable and reversible electrochemical redox properties of the HBPIs will enable them as promising pseudocapacitors [60]. Therefore, the galvanostatic charge-discharge (GCD) curves at different current densities and electrochemical impendence spectra (EIS) of the 6FDA-HBPI film were performed to investigate their potential capacitive properties. As shown in Figure 6a, the GCD tests showed two plateaus during the charging/discharging processes which are in consistence with the peaks in the CV experiments. The specific capacitance calculated from the discharged part of GCD

experiment is 69 F g^{-1} at a current density of 0.5 A g^{-1}. Compared with other similar materials reported in the literature [61-65], the capacitance value of 6FDA-HBPI is moderate. However, the capacitance of the polymers could be further enhanced by increasing the pore density of polymer films by physical or chemical modifications [66], which is currently underway in our lab. The EIS (frequency, 0.01-100000 Hz) was simulated using an equivalent circuit (Figure 6b). The Nyquist plots include a straight line in the low frequency region related to the ion diffusion process and a semicircle in the high frequency region derived from the interfacial charge-discharge resistance (R_{ct}). The impedance parameters of R_{ct} and double layer capacitance (C_{dl}) by fitting the experiment spectra with the equivalent circuit were found to be 86 Ω and 5.6×10^{-8} F. In view of the fact that the charge-discharge process accompanied with the color changes, these novel HBPIs may find an application as smart electrochromo-supercapacitors in the future.

Figure 6

4. Conclusion

In summary, we have readily synthesized two kinds of HBPIs with star-shaped triphenylamine *via* a facile route to introduce multiple redox species. In addition to the excellent solubility and thermal stability, the resulting HBPIs also exhibited multistage light modulations in vis/NIR regions. The electrochromic performances of these HBPIs revealed continuous modulation over the entire visible region, high electroactive reversibility, high optical contrast (63 % at 443 nm), low response time (2.6 s/1.9 s at 443 nm), high coloration efficiency (196 $cm^2 C^{-1}$ at 443 nm), outstanding stability and optical memory properties at once. On the other hand, the preliminary capacitive tests of the HBPI films demonstrated an acceptable specific capacitive value of 69 F g^{-1}. Considering these crucial factors mentioned above, the bifunctional HBPIs

with star-shaped triphenylamine are promising materials in the applications of electrochromic displays and electrochromo-supercapacitors. Overall, the comprehensive investigations of these HBPIs provide a deep understanding of their electro-optic effect, meanwhile paving the way for future intelligence applications.

Acknowledgments

Y. Yu thanks the Alexander von Humboldt Foundation for support in the form of the AvH-fellowship.

References

[1] G.F. Cai, J.X. Wang, P.S. Lee, Next-generation multifunctional electrochromic devices, Acc. Chem. Res. 49 (2016) 1469-1476.

[2] G.A. Niklasson, C.G. Granqvist, Electrochromics for smart windows: thin films of tungsten oxide and nickel oxide, and devices based on these, J. Mater. Chem. 17 (2007) 127-156.

[3] R.J. Mortimer, A.L. Dyer, J.R. Reynolds, Electrochromic organic and polymeric materials for display applications, Displays 27 (2006) 2-18.

[4] J. Remmele, D.E. Shen, T. Mustonen, N. Fruehauf, High performance and long-term stability in ambiently fabricated segmented solid-state polymer electrochromic displays, ACS Appl. Mater. Interfaces 7 (2015) 12001-12008.

[5] C. Ma, M. Taya, C. Xu, Smart sunglasses based on electrochromic polymers, Polym. Eng. Sci. 48 (2008) 2224-2228.

[6] V.K. Thakur, G.Q. Ding, J. Ma, P.S. Lee, X.H. Lu, Hybrid materials and polymer electrolytes for electrochromic device applications, Adv. Mater. 24 (2012) 4071-4096.

[7] H.T. Yu, S. Shao, L.J. Yan, H. Meng, Y.W. He, C. Yao, P.P. Xu, X.T. Zhang, W.P. Hu, W. Huang, Side-chain engineering of green color electrochromic polymer materials: toward adaptive camouflage application, J. Mater. Chem. C 4 (2016) 2269-2273.

[8] P.M. Beaujuge, J.R. Reynolds, Color control in π-conjugated organic polymers for use in electrochromic devices, Chem. Rev. 110 (2010) 268-320.

[9] Y.M. Zhang, X.J. Wang, W.R. Zhang, W. Li, X.F. Fang, B. Yang, M.J. Li, S.X.A. Zhang, A single-molecule multicolor electrochromic device generated through medium engineering, Light: Sci. Appl. 4 (2015) e249.

[10] X.J. Lv, W.J. Li, M. Ouyang, Y.J. Zhang, D.S. Wright, C. Zhang, Polymeric electrochromic materials with donor-acceptor structures, J. Mater. Chem. C 5 (2017) 12-28.

[11] L. Beverina, G.A. Pagani, M. Sassi, Multichromophoric electrochromic polymers: colour tuning of conjugated polymers through the side chain functionalization approach, Chem. Comm. 50 (2014) 5413-5430.

[12] J.A. Kerszulis, C.M. Amb, A.L. Dyer, J.R. Reynolds, Follow the yellow brick road: structural optimization of vibrant yellow-to-transmissive electrochromic conjugated polymers, Macromolecules 47 (2014) 5462-5469.

[13] Q. Ye, W.T. Neo, T. Lin, J. Song, H. Yan, H. Zhou, K.W. Shah, S.J. Chua, J.W. Xu, Pyrrolophthalazinedione (PPD)-based donor−acceptor polymers as high performance electrochromic materials, Polym. Chem. 6 (2015) 1487-1494.

[14] W.S. Li, Y.T. Guo, J.J. Shi, H.T. Yu, H. Meng, Solution-processable neutral green electrochromic polymer containing thieno[3,2‑b]thiophene derivative as unconventional donor units, Macromolecules 49 (2016) 7211-7219.

[15] T.L. Rose, S. D'Antonio, M.H. Jillson, A.B. Kon, R. Suresh, F. Wang, A microwave shutter using conductive polymers, Synth. Met. 85 (1997) 1439-1440.

[16] E.B. Franke, C.L.Trimble, J.S. Hale, M. Schubert, J.A. Woollam, Infrared switching electrochromic devices based on tungsten oxide, J. Appl. Phys. 88 (2000) 5777-5784.

[17] W.R. Lin, Y.J. Zheng, J. Zhang, X.H. Wan, Fabrication of core-shell nanostructures from near-infrared electrochromic amphiphilic diblock copolymers containing pendant dinuclear ruthenium group through assembly and their optical, electrochemical, and electroptical properties, Macromolecules 44 (2011) 5146-5154.

[18] J.A. Kerszulis, R.H. Bulloch, N.B. Teran, R.M.W. Wolfe, J.R. Reynolds, Relax: a sterically relaxed donor−acceptor approach for color tuning in broadly absorbing, high contrast electrochromic polymers, Macromolecules 49 (2016) 6350-6359.

[19] B.B. Cui, Y.W. Zhong, J.N. Yao, Three-state near-infrared electrochromism at the molecular scale, J. Am. Chem. Soc. 137 (2015) 4058-4061.

[20] B.B. Cui, J.H. Tang, J.N. Yao, Y.W. Zhong, A molecular platform for multistate near-infrared electrochromism and flip-flop, flip-flap-flop, and ternary memory, Angew. Chem. Int. Ed. 127 (2015) 9324-9329.

[21] A. Llordes, G. Garcia, J. Gazquez, D.J. Milliron, Tunable near-infrared and visible-light transmittance in nanocrystal-in-glass composites, Nature 500 (2013) 323-326.

[22] E.L. Runnerstrom, A. Llordes, S.D. Lounis, D.J. Milliron, Nanostructured electrochromic smart windows: traditional materials and NIR-selective plasmonic nanocrystals, Chem. Commun. 50 (2014) 10555-10572.

[23] T.E. Williams, C.M. Chang, E.L. Rosen, G. Garcia, E.L. Runnerstorm, B.L. Williams, B. Koo, R. Buonsanti, D.J. Milliron, B.A. Helms, NIR-Selective electrochromic heteromaterial frameworks: a platform to understand mesoscale transport phenomena in solid-state electrochemical devices, J. Mater. Chem. C 2 (2014) 3328-3335.

[24] A. Heckmann, C. Lambert, Organic mixed-valence compounds: a playground for electrons and holes, Angew. Chem. Int. Ed. 51 (2012) 326-392.

[25] M. Renz, K. Theilacker, C. Lambert, M. Kaupp, A reliable quantum-chemical protocol for the characterization of organic mixed-valence compounds, J. Am. Chem. Soc. 131 (2009) 16292-16302.

[26] H.J. Yen, G.S. Liou, Solution-processable novel near-infrared electrochromic aromatic polyamides based on electroactive tetraphenyl-p-phenylenediamine moieties, Chem. Mater. 21 (2009) 4062-4070.

[27] G.F. Cai, P. Darmawan, M.Q. Cui, J.X. Wang, J.W. Chen, S. Magdassi, P.S Lee, Highly Stable Transparent Conductive Silver Grid/PEDOT:PSS Electrodes for Integrated Bifunctional Flexible Electrochromic Supercapacitors, Adv. Energy Mater. 6 (2016) 1501882-1501889.

[28] P.P Zhang, F. Zhu, F.X Wang, J.H. Wang, R.H. Dong, X.D. Zhuang, O.G. Schmidt, X.L. Feng, Stimulus-Responsive Micro-Supercapacitors with Ultrahigh Energy Density and Reversible Electrochromic Window, Adv. Mater. 29 (2017) 1604491-1604497.

[29] T.G. Yun, D. Kim, Y.H. Kim, M. Park, S. Hyun, S.M. Han, Photoresponsive Smart Coloration Electrochromic Supercapacitor, Adv. Mater. 29 (2017) 1606728-1606737.

[30] G. Zhang, H. Bala, Y. Cheng, D. Shi, X. Lv, Q. Yu, P. Wang, High efficiency and stable dye-sensitized solar cells with an organic chromophore featuring a binary π-conjugated spacer, Chem. Commun. 16 (2009) 2198-2200.

[31] A. Mishra, M.K.R. Fischer, P. Bauerle, Metal-free organic dyes for dye-sensitized solar cells: from structure: property relationships to design rules, Angew. Chem. Int. Ed. 48 (2009) 2474-2499.

[32] F. Zhang, C. Yi, P. Wei, X.D. Bi, J.S. Luo, G. Jacopin, S.R. Wang, X.G. Li, Y. Xiao, S.M. Zakeeruddin, M. Gratzel, A novel dopant-free triphenylamine based molecular “butterfly” hole-transport material for highly efficient and stable perovskite solar cells, Adv. Energy Mater. 6 (2016) 1600401-1600407.

[33] Y. Shirota, Photo-and electroactive amorphous molecular baterials—molecular design, syntheses, reactions, properties, and applications, J. Mater. Chem. 15 (2005) 75-93.

[34] T. Kurosawa, T. Higashihara, M. Ueda, Polyimide memory: a pithy guideline for future applications, Polym. Chem. 4 (2013) 16-30.

[35] H.J. Yen, G.S. Liou, Solution-processable triarylamine-based high-performance polymers for resistive switching memory devices, Polym. J. 48 (2016) 117-138.

[36] H.J. Yen, G.S. Liou, Solution-processable triarylamine-based electroactive high performance polymers for anodically electrochromic applications, Polym. Chem. 3 (2012) 255-264.

[37] D. Weng, Y.C. Shi, J.M. Zheng, C.Y. Xu, High performance black-to-transmissive electrochromic device with panchromatic absorption based on TiO_2-supported viologen and triphenylamine derivatives, Org. Electron. 34 (2016) 139-145.

[38] S.W. Cai, H.L. Wen, S.H. Wang, H.J. Niu, C. Wang, X.K. Jiang, X.D. Bai, W. Wang, Electrochromic polymers electrochemically polymerized from 2, 5–dithienylpyrrole (DTP) with different triarylamine units: Synthesis, characterization and optoelectrochemical properties, Electrochim. Acta 228 (2017) 332-342.

[39] N.W. Sun, S.Y. Meng, D.M. Chao, Z.W. Zhou, Y.L. Du, D.M. Wang, X.G. Zhao, H.W. Zhou, C.H. Chen, Highly stable electrochromic and electrofluorescent dual-switching polyamide containing bis(diphenylamino)-fluorene moieties, Polym. Chem. 7 (2016) 6055-6063.

[40] C.W. Chang, G.S. Liou, S.H. Hsiao, Highly stable anodic green electrochromic aromatic polyamides: synthesis and electrochromic properties, J. Mater. Chem. 17 (2007) 1007-1015.

[41] G.S. Liou, H.Y. Lin, Synthesis and electrochemical properties of novel aromatic poly (amine−amide) s with anodically highly stable yellow and blue electrochromic behaviors, Macromolecules 42 (2009) 125-134.

[42] J.W. Cai, L.N. Ma, H.J. Niu, P. Zhao, Y.F. Lian, W. Wang, Near infrared electrochromic naphthalene-based polyimides containing triarylamine: Synthesis and electrochemical properties, Electrochim. Acta 112 (2013) 59-67.

[43] S. Abraham, G.P.T. Ganesh, S. Varughese, B. Deb, J. Joseph, Cross-linkable fluorene-diphenylamine derivatives for electrochromic applications, ACS Appl. Mater. Interfaces 7 (2015) 25424-25433.

[44] S.H. Hsiao, S.L. Cheng, New electroactive and electrochromic aromatic polyamides with ether-linked bis(triphenylamine) units, J. Polym. Sci. Part A: Polym. Chem. 53 (2015) 496-510.

[45] C. Quinton, V. Alain-Rizzo, C. Dumas-Verdes, F. Miomandre, G. Calvier, P. Audebert, Redox- and protonation-induced fluorescence switch in a new triphenylamine with six stable active or non-active forms, Chem. Eur. J. 21 (2015) 2230-2240.

[46] H.J. Yen, C.J. Chen, G.S. Liou, Flexible Multi‐Colored Electrochromic and Volatile Polymer Memory Devices Derived from Starburst Triarylamine‐Based Electroactive Polyimide, Adv. Funct. Mater. 23 (2013) 5307-5316.

[47] S.X. Xiong, P.T. Jia, K.Y. Mya, J. Ma, F. Boey, X.H. Lu, Star-like polyaniline prepared from octa (aminophenyl) silsesquioxane: enhanced electrochromic contrast and electrochemical stability, Electrochim. Acta 53 (2008) 3523-3530.

[48] A.P. Saxena, M. Deepa, A.G. Joshi, S. Bhandari, A.K. Srivastava, Poly (3,4-ethylenedioxythiophene)-ionic liquid functionalized graphene/reduced graphene oxide nanostructures: improved conduction and electrochromism, ACS Appl. Mater. Interfaces 3 (2011) 1115-1126.

[49] G.S. Liou, H.Y. Lin, H.J. Yen, Synthesis and characterization of electroactive hyperbranched aromatic polyamides based on A_2B-type triphenylamine moieties, J. Mater. Chem. 19 (2009) 7666-7673

[50] P.J. Flory, Molecular size distribution in three dimensional polymers. VI. Branched polymers containing A—R—Bf-1 type units, J. Am. Chem. Soc. (74) 1952 2718-2723.

[51] Y. Chen, Q.Y. Zhang, W.L. Sun, X.F. Lei, P. Yao, Synthesis and gas permeation properties of hyperbranched polyimides membranes from a novel (A2þB2B′þB2)-type method, J. Membr. Sci, 450 (2014) 138-146.

[52] C. Su, X.G. Zhu, L.H. Xu, N.N. Zhou, H.H. He, C. Zhang, Organic polytriphenylamine derivative-based cathode with tailored potential and its electrochemical performances, Electrochim. Acta, 196 (2016) 440-449.

[53] J.K. Bin, N.S. Cho, J.I. Hong, New Host Material for High‐Performance Blue Phosphorescent Organic Electroluminescent Devices. Adv. Mater. 24 (2012) 2911-2915.

[54] C.Q. Ma, M. Fonrodona, M.C. Schikora, M.M. Wienk, R.A.J. Janssen, P. Bauerle, Solution‐Processed Bulk‐Heterojunction Solar Cells Based on Monodisperse Dendritic Oligothiophenes, Adv. Funct. Mater. 18 (2008) 3323-3331.

[55] M.B. Robin, P. Day, Mixed valence chemistry-a survey and classification, Adv. Inorg. Radiochem. 10 (1968) 247-422.

[56] K. Karon, M. Lapkowski, A. Dabuliene, A. Tomkeviciene, N. Kostiv, J.V. Grazulevicius, Spectroelectrochemical characterization of conducting polymers from star-shaped carbazole-triphenylamine compounds, Electrochim. Acta, 154 (2015) 119–127.

[57] P. M. Beaujuge, S. Ellinger, J. R. Reynolds, The donor–acceptor approach allows a black-to-transmissive switching polymeric electrochrome, Nat. Mater. 7 (2008) 795-799.

[58] N.W. Sun, S.Y. Meng, Z.W. Zhou, J.N. Yao, Y.L. Du, D.M. Wang, X.G. Zhao, H.W. Zhou, C.H. Chen, High-contrast electrochromic and electrofluorescent dual-switching materials based on 2-diphenylamine-(9, 9-diphenylfluorene)-functionalized semi-aromatic polymers, RSC Adv. 6 (2016) 66288-66296.

[59] H. Zhao, Y.Y. Wei, J.S. Zhao, M. Wang, Three donor-acceptor polymeric electrochromic materials employing 2,3-bis(4-(decyloxy)phenyl)pyrido[4,3-b]pyrazine as acceptor unit and thiophene derivatives as donor units, Electrochim. Acta, 146 (2014) 231-241.

[60] G.P. Wang, L. Zhang, J.J. Zhang, A review of electrode materials for electrochemical supercapacitors, Chem. Soc. Rev. 41 (2012) 797-828.

[61] P.M. DiCarmine, T.B. Schon, T.M. McCormick, P.P. Klein, D.S. Seferos, Donor–Acceptor Polymers for Electrochemical Supercapacitors: Synthesis, Testing, and Theory, J. Phys. Chem. C 118 (2014) 8295-8307.

[62] D. Mo, W. Zhou, X. Ma, J. Xu, F. Jiang, D. Zhu, Alkyl functionalized bithiophene end-capped with 3 4-ethylenedioxythiophene units: synthesis, electropolymerization and the capacitive properties of their polymers, Electrochimica Acta 151 (2015) 477-488.

[63] A.M. Österholm, J.F. Ponder Jr., J.A. Kerszulis, J.R. Reynolds, Solution processed PEDOT analogues in electrochemical supercapacitors, ACS Appl. Mater. Interfaces 8 (2016) 13492-13498.

[64] Y.T. Guo, W.S. Li, H.T. Yu, D.F. Perepichka, H. Meng, Flexible Asymmetric Supercapacitors via Spray Coating of a New Electrochromic Donor–Acceptor Polymer, Adv. Energy Mater. 7 (2017) 1601623-1601629.

[65] X.C. Li, Y.Z. Zhang, C.Y. Wang, Y. Wan, W.Y. Lai, H. Pang, W. Huang, Redox-active triazatruxene-based conjugated microporous polymers for high-performance supercapacitors, Chem. Sci. 8 (2017) 2959–2965.

[66] M.X. Sun, P.X. Kuang, L.Q. Qin, C. Gu, Z.Q. Xie, Y.G. Ma, In situ synthesis of electroactive conjugated microporous fullerene films capable of supercapacitive energy storage, Chem. Commun. 53 (2017) 9602-9605.

Scheme 1 Synthesis of the triamine with star-shaped triphenylamine.

Scheme 2 Synthesis of HBPIs.

Figure 1 Design concept of HBPIs with star-shaped triphenylamine.

Figure 2 ^{1}H NMR spectra of trinitro (a) and triamine (b) monomers.

Figure 3 CV diagrams of trinitro (a), triamine (b) and HBPI thin films coated on ITO glass slide (c) in 0.1 M TBAP/CH_3CN at a scan rate of 50 mV/s. (d) CV diagrams of 6FDA-HBPI thin film coated on ITO glass slide over 5000 cyclic scans for the first two redox processes in 0.1 M TBAP/CH_3CN at a scan rate of 50 mV/s. (e) Presumptive order of oxidation reactions in the star-shaped triphenylamine segment of the model compound. (f) Calculated molecular orbitals of the model compound (TD-DFT method at the B3LYP/6-31G (d, p)).

Figure 4 (a) Colors of 6FDA-HBPI film at different potentials. (b) UV-vis-NIR spectroelectrochemistry of 6FDA-HBPI thin film coated on an ITO glass slide in 0.1M TBAP/CH_3CN at different applied potentials from 0.0 to 1.3 V. (c) CIE 1931chromaticity diagram of 6FDA-HBPI at different potentials.

Figure 5 Electrochromic switching of 6FDA-HBPI thin film coated on the ITO glass slide in 0.1 M TBAP/CH_3CN with a cycle time of 20 s. (a) Optical switching between 0.00 V and 0.60 V with the wavelength monitored at 443 nm; (b) Optical switching between 0.00 V and 0.80 V with the wavelength monitored at 446 nm; (c) Optical switching between 0.00 V and 1.10 V with the wavelength monitored at 520 nm; (d) Optical switching between 0.00 V and 1.30 V with the wavelength monitored at 600 nm.

Figure 6 (a) Galvanostatic charge-discharge curves of 6FDA-HBPI film in a three-electrode configuration at different current densities. (b) Impendence spectra of 6FDA-HBPI film (inset: the equivalent circuit diagram).

Table 1 Molecular Weights and Solubilities of the HBPIs.

	GPC[a]			Solvents[b]						
Sample	M_w	M_n	PDI	NMP	DMAc	DMF	DMSO	THF	$CHCl_3$	CH_3CN
ODPA-	53000	26100	2.03	++	++	++	++	+-	+-	--
6FDA-	63700	30800	2.07	++	++	++	++	++	++	--

[a] Relative to polystyrene standard, using DMF as the eluent; [b] Qualitative solubilities were tested with 10 mg of polymers in 1mL of solvent. ++, soluble at room temperature; +-, partially soluble; --, insoluble even on heating.

Table 2 Optical and electrochemical properties of the HBPIs.

polymer	Solution(nm)[a]	Film(nm)		Oxidation Potional(V)[b]					E_g[c]	HOMO[d]	LUMO[e]
	λ_{max}	λ_{onset}	λ_{max}	E_{onset}	$E_{1/2}$ 1st	2nd	3rd	4th			
ODPA-HBPI	315,345	430	314,352	0.34	0.46	0.72	0.98	1.23	2.88	4.78	1.90
6FDA-HBPI	303,339	433	305,343	0.33	0.46	0.72	0.99	1.24	2.86	4.77	1.91

[a] The polymer concentration was 1×10^{-5} mol/L in NMP. [b] From CV vs. Ag/AgCl; $E_{1/2}$ (Average potential of the redox couple peaks). [c] The data were calculated by the equation: $E_g = 1240/\lambda_{onset}$ (energy gap between HOMO and LUMO). [d] The HOMO energy levels were calculated from CV and were referenced to ferrocene (4.8 eV; $E_{onset} = 0.36$ V). [e] LUMO = HOMO- E_g.

Table 3 Electrochromic properties of the 6FDA-HBPI.

Switching potentials (V)	$\lambda_{monitored}$ (nm) [a]	Response time (s) [b]	Δ%T	CE (cm^2 C^{-1}) [c]
0.00-0.60	443	2.6/1.9	63	196
0.00-0.80	446	1.8/4.3	42	92
0.00-1.10	520	2.3/1.8	44	86
0.00-1.30	600	4.9/3.1	49	89

[a] Wavelength monitored in the electrochromic switching processes. [b] The coloring/blenching time for 90% of the total transmittance change. [c] Coloration efficiency is derived from the equation: $CE = \Delta OD/Q_d$, $\Delta OD = \log(T_{blenched}/T_{colored})$.

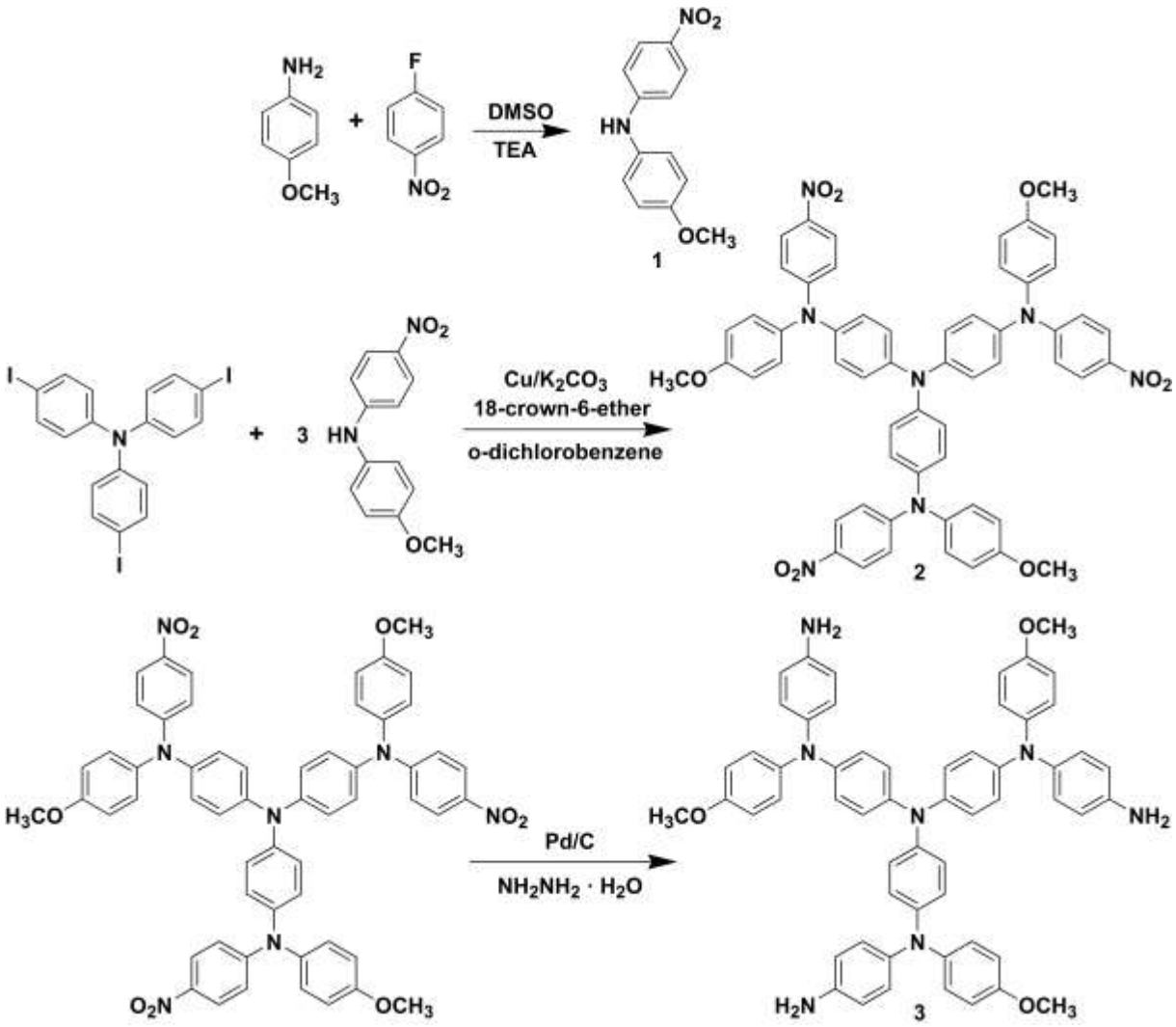

Scheme 1

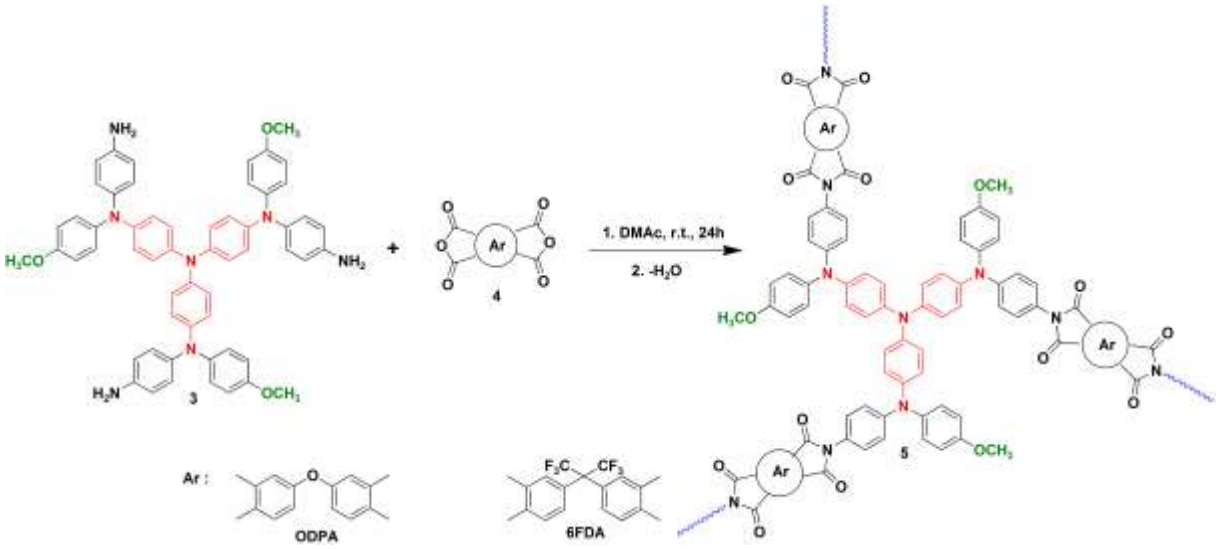

Scheme 2

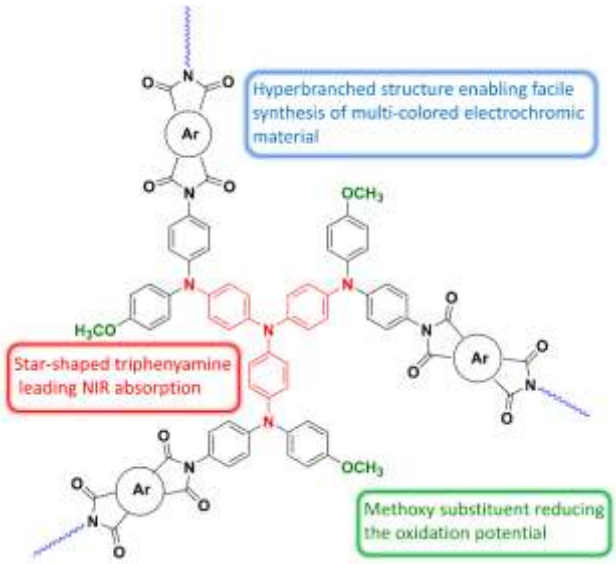

Figure 1

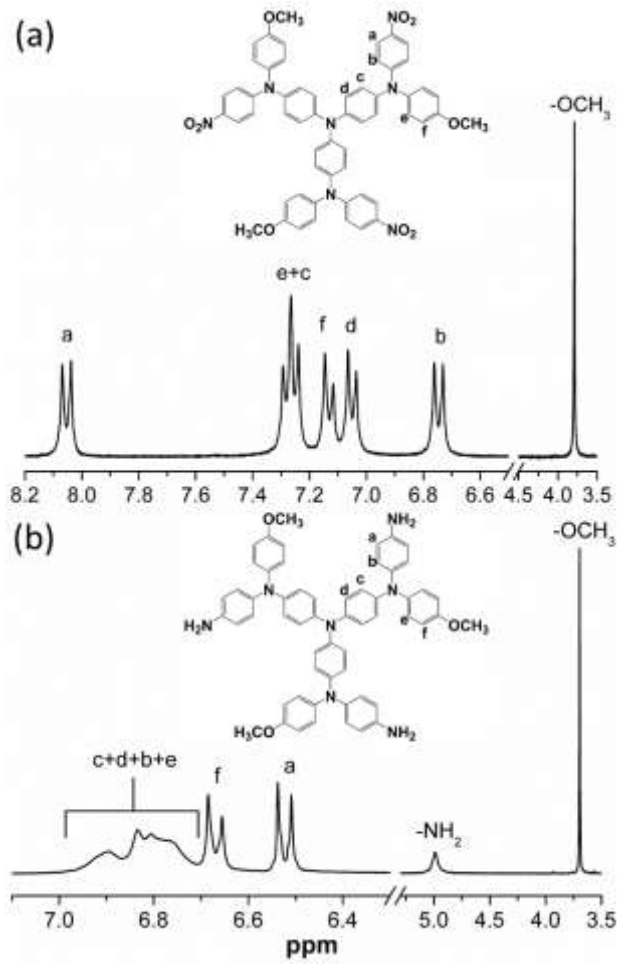

Figure 2

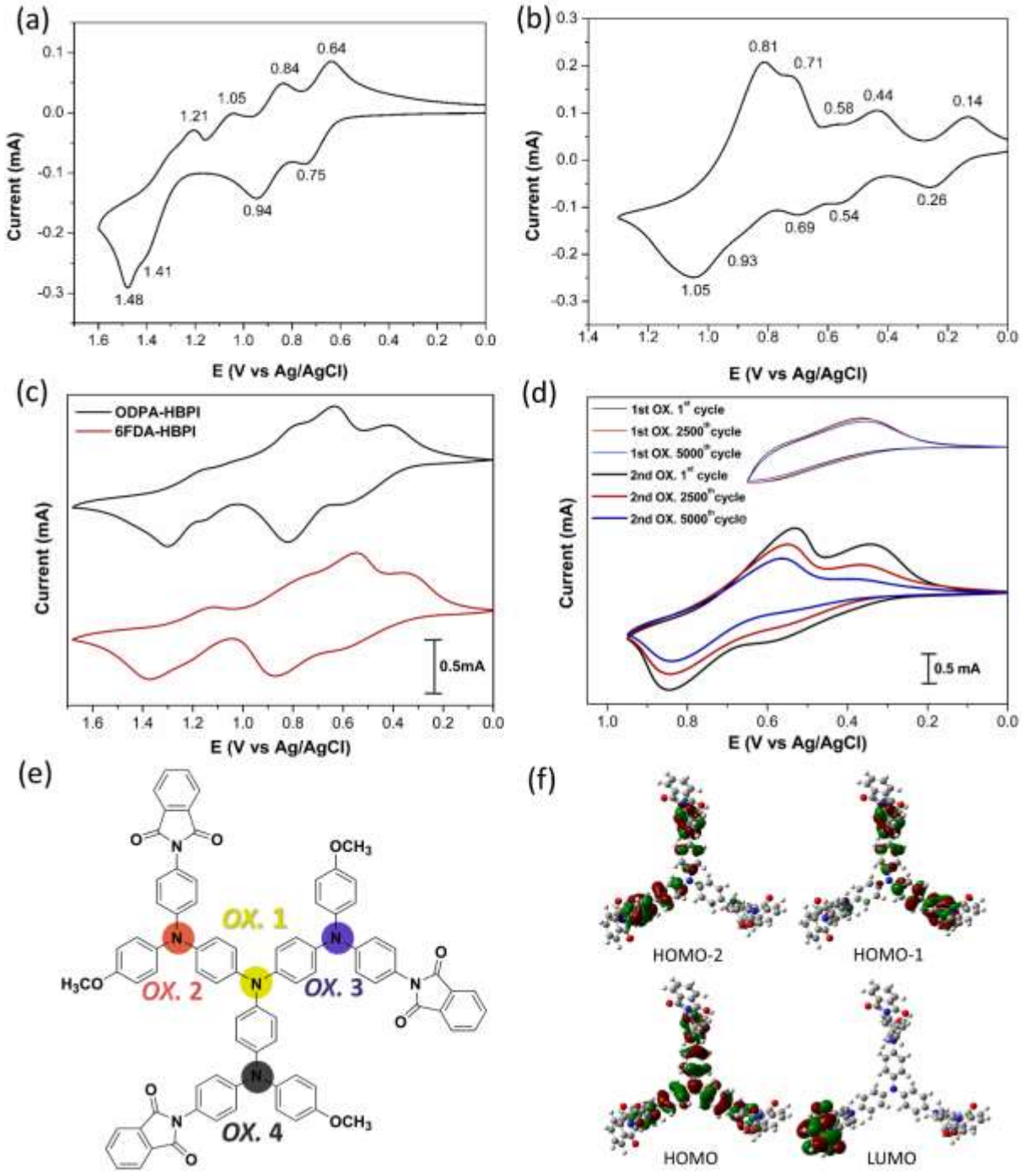

Figure 3

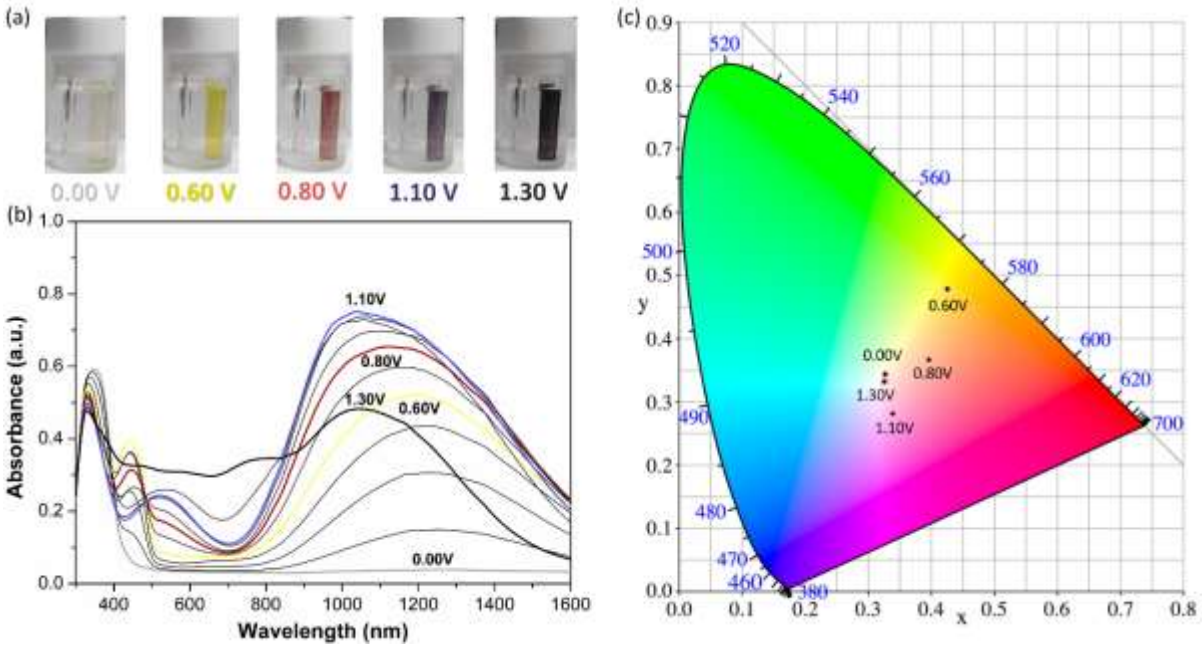

Figure 4

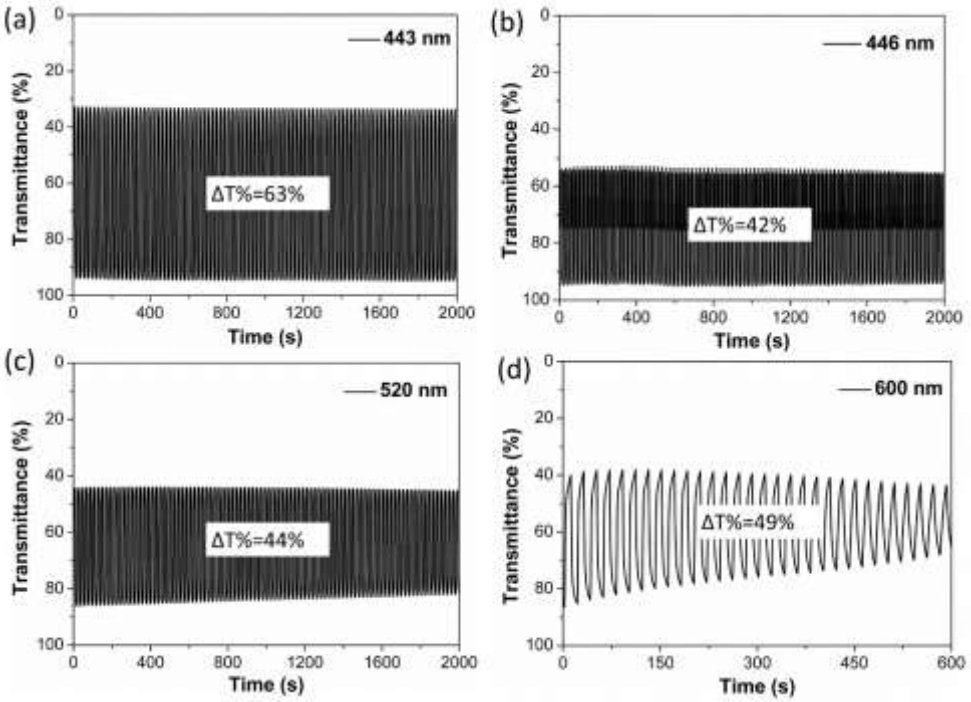

Figure 5

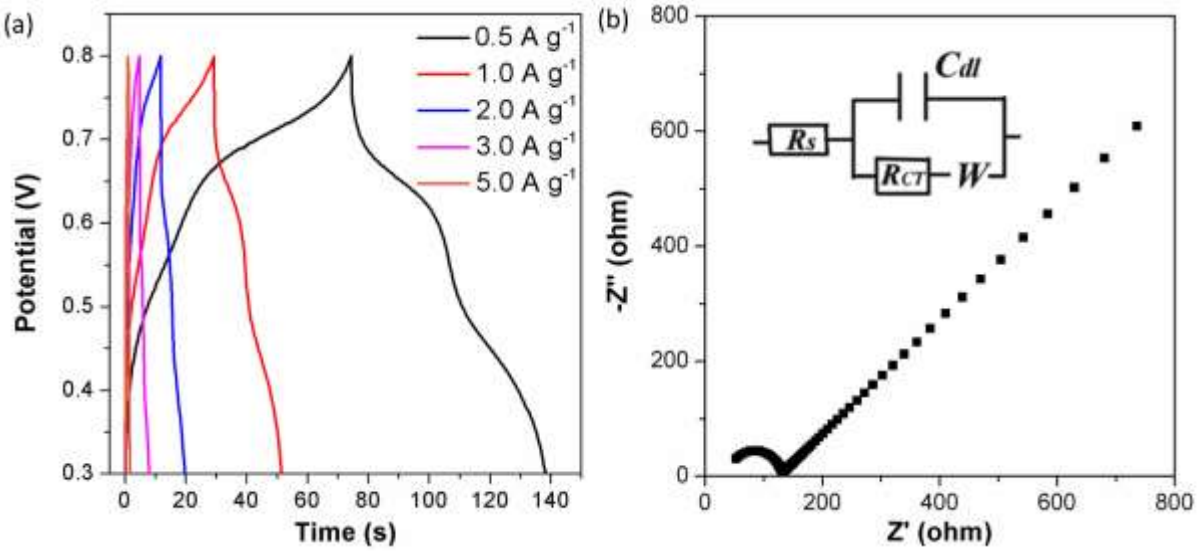

Figure 6